Enhanced mechanical energy conversion with selectively decayed wood

Journal Article

Author(s):
Sun, Jianguo; Guo, Huizhang; Schädli, Gian Nutal; Tu, Kunkun; Schär, Styfen; Schwarze, Francis W.M.R.; Panzarasa, Guido; Ribera, Javier; Burgert, Ingo

Publication date:
2021

Permanent link:
https://doi.org/10.3929/ethz-b-000475529

Originally published in:
Science Advances 7(11), https://doi.org/10.1126/sciadv.abd9138

APPLIED SCIENCES AND ENGINEERING

Enhanced mechanical energy conversion with selectively decayed wood

Jianguo Sun[1,2], Huizhang Guo[1,2], Gian Nutal Schädli[3], Kunkun Tu[1,2], Styfen Schär[1], Francis W.M.R. Schwarze[4], Guido Panzarasa[1,2], Javier Ribera[4]*, Ingo Burgert[1,2]*

Producing electricity from renewable sources and reducing its consumption by buildings are necessary to meet energy and climate change challenges. Wood is an excellent "green" building material and, owing to its piezoelectric behavior, could enable direct conversion of mechanical energy into electricity. Although this phenomenon has been discovered decades ago, its exploitation as an energy source has been impaired by the ultralow piezoelectric output of native wood. Here, we demonstrate that, by enhancing the elastic compressibility of balsa wood through a facile, green, and sustainable fungal decay pretreatment, the piezoelectric output is increased over 55 times. A single cube (15 mm by 15 mm by 13.2 mm) of decayed wood is able to produce a maximum voltage of 0.87 V and a current of 13.3 nA under 45-kPa stress. This study is a fundamental step to develop next-generation self-powered green building materials for future energy supply and mitigation of climate change.

INTRODUCTION

Buildings account for about 40% of worldwide energy consumption and for nearly one-quarter of global greenhouse gas emissions (*1*–*3*). Boosting the building energy efficiency plays an increasingly decisive role to meet future energy and climate targets (*4*, *5*). Current efforts mainly focus on the reduction of building energy consumption through the design of envelopes for enhancing insulation, sun shading, and natural ventilation (*6*–*8*). Besides reducing energy consumption, the integration of green renewable energy sources into the building architecture is of crucial importance to make them energy-neutral or even energy-producing entities (*9*, *10*). Current technology focuses predominantly on photovoltaics (PV), which produces electricity for buildings by transforming sunlight. However, the energy gain is highly dependent on weather conditions, and solar panel installation does not pay off for all kinds of buildings (*2*, *11*–*13*). Installation of solar panels influences the aesthetic appearance of buildings architecture, in particular, when larger PV devices are integrated on the roofs. Therefore, it is highly desirable that raw construction materials such as wood, concrete, or glass would be able to produce electricity from renewable sources without any weather restrictions. Only then could future buildings generate their own electricity without limitations while maintaining their aesthetic appearance.

Wood is a traditional building material, whose use is increasing thanks to its notable sustainability and advantages originating from being a renewable and CO_2 storing resource (*8*, *14*). Beyond that, wood might even be exploited to contribute to power generation in buildings. Wood cell walls are mainly composed of cellulose, hemicelluloses, and lignin. The cellulose consists of amorphous and crystalline regions. Piezoelectricity in wood is induced by the displacement of crystalline cellulose in response to applied mechanical stress, resulting in the generation of electrical charges. This phenomenon was discovered decades ago (*15*–*17*). However, progresses in using wood as an energy convertor have been hindered owing to the low piezoelectric moduli and the limited deformability of wood itself, resulting in an inefficient electrical output (*16*).

Throughout history, wood decay by fungi has been a considerable detriment for the durability of wood in building construction (*18*–*23*). Here, we take advantage of this commonly undesired decay process to partially remove lignin and hemicellulose from balsa wood, using the white rot fungus *Ganoderma applanatum* (Empa 646), resulting in biologically modified wood with enhanced compressibility (*24*–*26*). In previous studies, the poor deformability of wood resulted in small piezoelectric effects due to its insufficient deformation under a minute (e.g., tens of kilopascals) load (*27*, *28*). In a recent study (*29*), we have shown that a chemical delignification treatment can enhance the deformability of wood, resulting in an increased piezoelectric output. Here, we explore a biological method and demonstrate that wood deformability and, consequently, the displacement of cellulose crystals even under minute loads can be successfully achieved by taking advantage of a completely natural fungal decay process, without the need of using chemicals. By applying this highly sustainable method, we were able to fabricate an efficient wood energy convertor with a 55 times increment in piezoelectric effect. Our results provide previously unknown inputs for the comprehension of wood piezoelectricity and the development of its applications. Such green, biocompatible, biodegradable, and cost-effective decayed wood may become a useful point-of-use power supply in future sustainable buildings (*1*, *30*–*34*).

RESULTS

Balsa (*Ochroma pyramidale* Cav. ex Lam.) wood with high porosity and low density (about 94.8 kg/m^3) was incubated with the white rot fungus *G. applanatum* for 4 to 12 weeks. After fungal treatment, the decayed wood had improved compressibility due to structural alterations. The second row in Fig. 1 illustrates the general working principle of wood piezoelectricity, which originates from crystalline cellulose. Upon compression of the crystalline cellulose segments, centroids of positive charges and negative charges no longer coincide, inducing charges on the surfaces of wood for electrostatic equilibrium. A higher compressibility of the wood, thanks to the

[1]Wood Materials Science, Institute for Building Materials, ETH Zürich, 8093 Zürich, Switzerland. [2]WoodTec Group, Cellulose & Wood Materials, EMPA, 8600 Dübendorf, Switzerland. [3]Institute for Biomechanics, Department of Health Sciences and Technology, ETH Zürich, 8093 Zürich, Switzerland. [4]Laboratory for Cellulose & Wood Materials, EMPA, 9014 St. Gallen, Switzerland.
*Corresponding author. Email: iburgert@ethz.ch (I.B.); javier.ribera@empa.ch (J.R.)

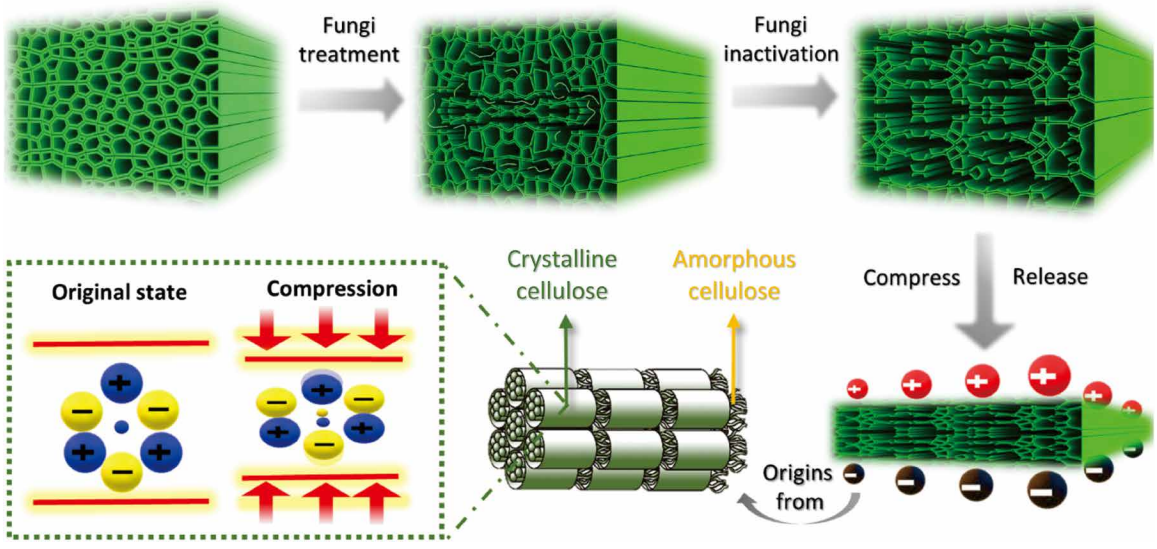

Fig. 1. Graphical illustration of the structure evolution of wood upon fungal treatment.

fungal treatment, results in a higher displacement of cellulose crystals, which enhances the electrical output. The hyphae, i.e., the thread-like cells of the fungus (fig. S1), grow within the wood cell lumen and secrete extracellular enzymes able to degrade lignin, resulting in changes of the wood structure (Fig. 1). Balsa, thanks to its lignin composition, is attacked by the selected white rot fungi more easily than other wood species (such as spruce, pine, and fir), resulting in a significantly reduced delignification time (*35*, *36*).

The influence of the fungal treatment on the morphology and structure of balsa wood was analyzed in detail on transverse sections by scanning electron microscopy (SEM). As shown in Fig. 2A, the native wood (0% weight loss) has a honeycomb-like porous structure and cell lumina with dimensions of 20 to 50 μm and thin cell walls. Weight loss caused by *G. applanatum* during incipient stages of decay (after 4 weeks) is around 15%. As shown in Fig. 2 (B and C), the wood structure changes are hardly visible after 4 weeks of exposure to *G. applanatum*. Structural changes become more evident when the weight loss increases to 25 and 35% after 6 and 8 weeks of fungal colonization, respectively (Fig. 2, D to F). In the wood sections highlighted by green frames, several cell walls are destroyed while others appear to be unaltered, indicating an inhomogeneous lignin degradation throughout the balsa wood in these two stages. The destruction of cell walls appears even more obvious in SEM images taken at higher magnification (Fig. 2F and fig. S2). After 10 weeks, balsa wood was strongly decayed, with a weight loss of 45%. As indicated in Fig. 2G, most of the cell walls are destroyed, forming large spaces between the rays. This structural alteration is responsible for the high mechanical compressibility of fungal treated wood. Excessive degradation with weight losses (50, 55, and 60%) results in a loss of the original shape of the balsa wood blocks, even without being compressed (Fig. 2, H and I, and fig. S3). The optimum weight loss of wood was determined to be approximately 45%, as it allows retaining the shape of the wood, but accelerating compressibility.

The weight loss evolution over time for wood incubated with *G. applanatum* is provided in Fig. 2J. Weight losses increased from 15 to 25, 35, 45, and 55% after an exposure time of 4 to 6, 8, 10, and 12 weeks, respectively. We also investigated the effect of two other white rot fungi (*Phanerochaete chrysosporium*, Empa 605; and *Ganoderma adspersum*, Empa 033) on balsa wood, but the decay rate was much lower compared to that obtained with *G. applanatum* (see table S1). Fourier transform infrared (FTIR) spectroscopy analysis of native wood and decayed wood (45% weight loss) was carried out to check partial removal of lignin and hemicelluloses (Fig. 2K). A decrease and shift in the relative intensities of characteristic lignin bands at 1594, 1503, and 1460 cm^{-1} are indicative of preferential lignin degradation by *G. applanatum*, as expected (*37*). Decline in the relative intensities of bands at 1736 cm^{-1} indicated that *G. applanatum* also affected the hemicellulose fraction. X-ray diffraction (XRD) patterns of native wood and decayed wood with 45% weight loss show characteristic diffraction peaks at 14.8° (1 to 10), 16.5° (110), and 22.5° (200) of both native wood and decay wood, indicating that cellulose Iβ crystalline structure of the native wood was not altered during the degradation process (fig. S4).

As shown in Fig. 3A, the decayed wood (45% weight loss) shows a high mechanical compressibility along the tangential direction and can recover to the original state after release of the stress, in sharp contrast to the rigid native wood. To further evaluate the mechanical properties of balsa wood before and after fungal treatment, we carried out multiple compression measurements. Figure 3B compares the mechanical compressibility of wood for different weight losses, varying from 0 to 45%. Under a stress load of 45 kPa (about 10-N force), the native wood only shows a small strain load of approximately 0.44%. When the weight loss increases to 15, 25, 35, and 45%, the strain load in the decayed wood increases by 2.71, 11.12, 18.64, and 23.67%, respectively. In comparison to native wood, decayed wood with a 15% weight loss shows a slight improvement in compressibility, while more marked changes can be seen at a higher weight loss. For instance, a 54 times strain increase, compared to native state, was obtained when the weight loss of balsa wood was 45%. This wood compression behavior for different weight losses is based on the structural changes caused by the fungus, as shown by the SEM images in Fig. 2.

As decayed wood with 45% weight loss showed the best compressibility performance, its compression behavior was further evaluated at different stress levels (Fig. 3C). Higher stresses result in higher strain. Compared to the curves for a load of up to 20 and 45 kPa

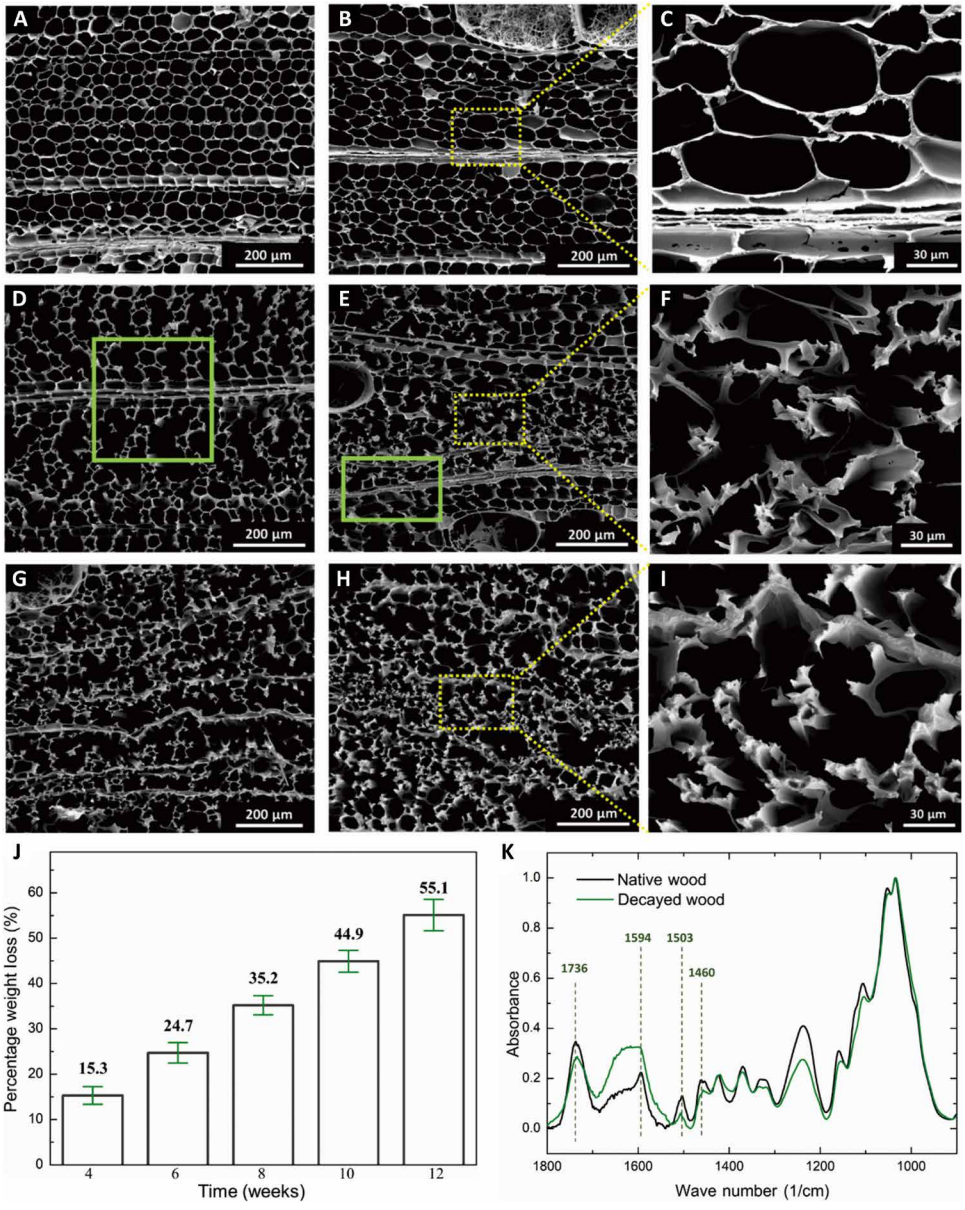

Fig. 2. SEM images of wood decayed by *G. applanatum* (transverse sections) showing different weight loss. (**A**) Zero percent weight loss (native wood). (**B**) Fifteen percent weight loss. (**C**) High-magnitude SEM image of wood with 15% weight loss. (**D**) Twenty-five percent weight loss. (**E**) Thirty-five percent weight loss. (**F**) High-magnitude SEM image of wood with 35% weight loss. (**G**) Forty-five percent weight loss. (**H**) Fifty-five percent weight loss. (**I**) High-magnitude SEM image of wood with 55% weight loss. (**J**) Increase in weight loss of balsa wood by *G. applanatum* over time. Error bars indicate SDs for 15 sets of data points. (**K**) FTIR spectra of the native wood and decayed wood with 45% weight loss.

(black and red curves, respectively), the stress-strain curve for a maximum stress of 100 kPa (blue curve) indicates a different behavior. All curves show a viscoelastic behavior with a short initial linear phase followed by an exponential increase. While the curves loaded until a stress level of 20 and 45 kPa remain in this phase, the loading to 100 kPa leads to a third phase with an almost linear increase. Although it is difficult to extract the underlying structure-property relationships to explain this behavior, the comparison of the three curves allows drawing some conclusions on the impact of the maximum stress levels. The curve obtained with a loading of 100 kPa shows a much higher energy dissipation than the other two curves, indicating that there is a stress limit for repeating loading events, which is around 45 to 50 kPa for these samples. In previous research, chemical approaches involving, e.g., sodium chlorite, sodium hydroxide, or acetic acid/hydrogen peroxide, have been used to remove lignin and hemicellulose from wood (*29*, *38*). Such methods are faster and more efficient than the use of white rot fungi and could result in more compressible wood structures. However, these merits of chemical delignification approaches are outweighed by the fundamental advantage of our fungi-based method: that is, to be fully sustainable and environment friendly.

To evaluate the mechanical stability of fungal decayed wood (45% weight loss), a cyclic compression test was performed at a constant stress of 45 kPa. As shown in Fig. 3D, only small plastic deformations

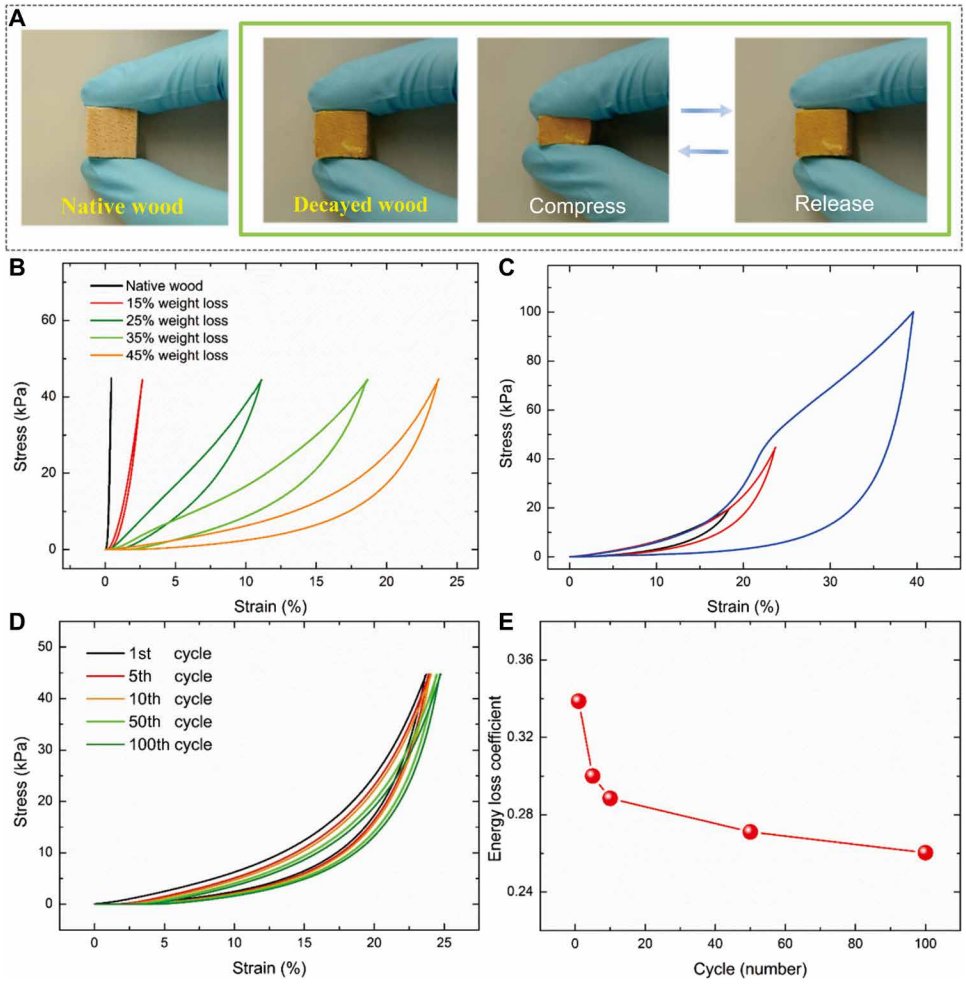

Fig. 3. Mechanical properties of balsa wood before and after fungal treatment. (**A**) Photographs of the decayed wood showing its higher and reversible compressibility compared to native wood. (**B**) Stress-strain curves of the decayed wood with different weight losses. (**C**) Stress-strain curves of the decayed wood (45% weight loss) under compression with different maximum stresses of 20, 45, and 100 kPa, respectively. (**D**) Stress-strain curves of the decayed wood (45% weight loss) under cyclic compression at a constant stress of 45 kPa. (**E**) Energy loss coefficient of the decayed wood during different cycles derived from the stress-strain curves in (D). Photo credit: Jianguo Sun, ETH Zürich.

occurred after 100 loading-unloading cycles, showing the good mechanical stability of the decayed wood. This can be further demonstrated by the energy dissipation in different cycles. As shown in Fig. 3E, the energy loss decreases from 0.34 in the 1st cycle to 0.26 for the 100th cycle, which is relatively low compared to other materials with high compressibility (*39*, *40*). The good mechanical compressibility and stability of the decayed wood was attributed to the unique structure generated by the fungal treatment.

The piezoelectric output was measured by a programmable electrometer (Keithley 6514). A linear motor, which could place a defined pressure on the samples at constant frequency, was used to compress the wood blocks. Figure S5 illustrates the piezoelectric output measurement setup. The open-circuit voltage instantaneously generated by native wood under a constant stress of 45 kPa was as small as 0.015 V, with heavy noise (fig. S6). As shown in Fig. 4A, decayed wood with 15% weight loss shows a slight improvement in voltage output when compared to native wood, but only rising up to 0.085 V. When the weight loss was increased to 25, 35, and 45%, the voltage of decayed wood reached up to 0.33, 0.59, and 0.87 V, the highest voltage increment being of 58 times compared to native wood. The growing voltage was ascribed to the increasing mechanical compressibility of decayed wood, which is linked to the increase in weight loss. This was further confirmed by measuring the associated short-circuit current produced by these samples, shown in fig. S7. A long-term compression/releasing test was conducted to confirm the mechanical durability of this decayed wood with 45% weight loss under a constant stress of 45 kPa. As is shown in Fig. 4B, the output voltage was maintained at about 0.84 V with minor fluctuations up to 500 cycles and no visible decline, indicating high structural robustness. The maximum current of 13.3 nA was generated by the decayed wood with a weight loss of 45%, two orders of magnitude higher than that of native wood, which is similar to voltage output (Fig. 4C). Furthermore, the electrical output of decayed wood (45% weight loss) was measured under different stress levels. As shown in Fig. 4D and fig. S8, for the same sample, a higher mechanical stress resulted in a higher electrical output and a maximum current of 19 nA (voltage 1.32 V) that was generated under the highest stress of 100 kPa. The corresponding compression force applied on

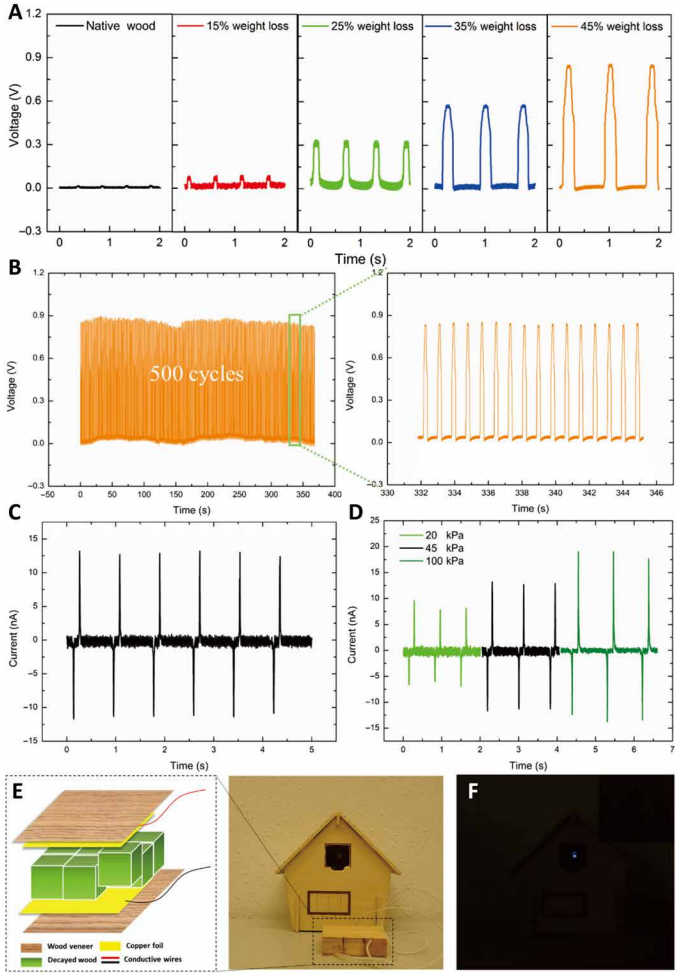

Fig. 4. Electrical output of decayed wood. (**A**) Output voltage of the decayed wood with different weight loss. (**B**) Voltage of decayed wood (45% weight loss) under cyclic compression test for 500 cycles. (**C**) Current of the decayed wood (45% weight loss) under a constant stress of 45 kPa. (**D**) Output current of the decayed wood (45% weight loss) under compression with different maximum stress of 20, 45, and 100 kPa, respectively. (**E** and **F**) Application of the decayed wood multicube prototype for powering a commercial LED in a house model. Photo credit: Jianguo Sun, ETH Zürich.

the wood surface was recorded by the loading cell mounted on the linear motor, as shown in fig. S8.

The piezoelectric effect in wood results from the mechanical deformation of crystalline cellulose whose unit cell is similar to monoclinic symmetry class 2 (2 is the twofold symmetry axis). When the twofold symmetry axis of the crystal lattice (longitudinal axis of the molecules) is parallel to the z axis, the piezoelectric tensor for this crystal can be written as

$$\begin{matrix} 0 & 0 & 0 & d_{14} & d_{15} & 0 \\ 0 & 0 & 0 & d_{24} & d_{25} & 0 \\ d_{31} & d_{32} & d_{33} & 0 & 0 & d_{36} \end{matrix}$$

Thus, eight piezoelectric moduli should exist in wood, including d_{14}, d_{15}, d_{24}, d_{25}, d_{13}, d_{32}, d_{33}, and d_{36} (*15*). However, almost all the previous research only reported the existence of d_{14} and d_{25} moduli in wood, representing polarization in the x direction produced by shear stress in the yz plane and polarization in the y direction induced by shear stress in the zx plane, respectively. For our samples, it is reasonable to assume that the d_{25} modulus could be present as well, as the fiber misalignment in balsa wood leads to the formation of shear stresses under compression (fig. S9) (*41*, *42*). Besides, the distortion of cellulose fibers induced by mechanical compression could also activate another piezoelectric modulus, the d_{32} one (*43*). The increased piezoelectric effect observed in decayed wood could then result from the contribution of different piezoelectric moduli, induced by the enhanced displacement of cellulose crystals in the highly compressible wood structure. In previous studies, powerful tools have been used to investigate the mechanisms of piezoelectric effects, such as Kelvin probe force microscopy (*44*) and COMSOL Multiphysics simulations (*45*), of molecular (*46*, *47*) and structural levels. However, these methods have not yet been tested on a complex, hierarchical matrix such as our decayed wood. Hence, further investigations are needed to obtain a better understanding of the piezoelectric mechanisms of the decayed wood.

Because the electrical output of a single piece [15 mm (L) by 15 mm (R) by 13.2 mm (T)] of decayed wood is limited, the electrical output of two decayed wood cubes connected in series or parallel was tested to demonstrate scalability. As is shown in fig. S10, while the individual voltage output of two single wood cubes was about 0.87 and 0.84 V, respectively, the output voltage of the cubes connected in series could reach 1.7 V. The maximum current produced by two individual decayed wood cubes was about 13 nA. Once they were connected in parallel, the current was increased to 26 nA. These results indicate that the voltage and current can be improved simply by integrating more wood cubes in different electrical connection modes, depending on the desired applications. To further demonstrate the upscaling potential and feasibility for future building applications, we fabricated a simple prototype of wood floor composed of nine parallel connected wood blocks, all with similar weight losses of 45%. As illustrated in Fig. 4E, two pieces of copper foil with a size of 45 mm by 45 mm were attached onto the radial sections of the decayed wood blocks and were then covered with two pieces of wood veneer (500-μm thickness). Conductive wires were led out and connected to a commercial light-emitting diode (LED), fixed behind the window of a small wood model house. The LED could be switched on directly by repeatedly and strongly pressing a hand on the demonstrator. Both the compressing and releasing action of the hand can light up the LED, while no light shines during the holding process, as shown in Fig. 4E and the inset pictures. Figure S11 shows that the current generated by the combined elements under flapping hands was increased to 150 nA, indicating the potential feasibility of application as power supply in wood floorings of future buildings. On the basis of our fundamental study, we envision the possibility to make large-scale wood floorings, allowing the production of electricity from human activities, such as in ballrooms.

DISCUSSION

In summary, we have demonstrated a facile, nontoxic, low-cost, and eco-friendly approach to functionalize wood for efficiently the production of electricity from mechanical energy input. Compared to established chemical delignification protocols, we have taken advantage of a natural, usually unwanted, fungi decay to partially remove lignin and hemicelluloses from native balsa wood to achieve a highly compressible wood structure. Thanks to this compressibility,

leading to an increased displacement of cellulose crystals, the partially degraded balsa wood displayed an enhanced piezoelectric effect. This renewable, biocompatible, economical, and eco-friendly decayed wood [15 mm (L) by 15 mm (R) by 13.2 mm (T)] can produce voltage and current of 0.87 V and 13.3 nA under a low pressure of 10 N, which is over 55 times the output of native wood. Decayed wood blocks connected in parallel or series to produce larger elements could generate higher current or voltage and be used to run low-power electronics, indicating the feasibility of application in future buildings. This study opens new possibilities to use renewable and sustainably processed materials for the design of future buildings with higher energy efficiency thanks to the ability to produce their own electricity through various indoor human activities.

MATERIALS AND METHODS

Decayed wood preparation with *G. applanatum*

Seventy-five wood samples of *O. pyramidale* (Balsa) with dimensions of 15 mm (T) by 15 mm (R) by 15 mm (L) were oven dried at 103°C for 24 hours to record initial dry weight. Samples were sterilized with ethylene oxide (Sigma-Aldrich, Buchs, Switzerland) and then placed into Kolle culture flasks containing freshly inoculated *G. applanatum* (Empa 646) growing on 75 ml of sterilized (20 min at 121°C) 4% Malt Extract Agar (MEA) (Oxoid, Platern, Switzerland). Fifteen biological replicates per incubation conditions were studied. All cultures were maintained in the dark at 22°C and 70% relative humidity. After different incubation periods (4, 6, 8, 10, and 12 weeks), the fungal biomass was carefully removed from the wood surfaces with a brush and the final weight was recorded after drying the samples in the oven at 103°C for 24 hours. It is noteworthy that there is a small shrinkage in the tangential direction of the bulk wood after fungal treatment (fig. S12).

Decayed wood preparation with other fungi

Fifteen wood samples of *O. pyramidale* (Balsa) with dimensions of 15 mm (T) by 15 mm (R) by 15 mm (L) were oven dried at 103°C for 24 hours to record initial dry weight. Samples were sterilized with ethylene oxide (Sigma-Aldrich, Buchs, Switzerland) and then placed into Kolle culture flasks containing freshly inoculated *P. chrysosporium* (Empa 605) and *G. adspersum* (Empa 003) growing on 75 ml of sterilized (20 min at 121°C) 4% MEA (Oxoid, Pratteln, Switzerland). Five biological replicates per incubation conditions were studied. All cultures were maintained in the dark at 22°C and 70% relative humidity. After different incubation periods (4, 8, and 12 weeks), the fungal biomass was carefully removed from the wood surfaces with a brush and the final weight was recorded after drying the samples in the oven at 103°C for 24 hours.

Assembly of wood cubes

Nine wood blocks with similar weight losses of 45% were connected in parallel. Then, two pieces of copper foil with a size of 45 mm by 45 mm were attached onto the radial sections of the decayed wood blocks and covered with two pieces of wood veneer (500-μm thickness each). Conductive wires were led out between the copper foil and wood veneer.

Microtome cutting

The samples surfaces characterized by SEM (FEI Quanta 200F) were prepared using a rotary microtome (Leica Ultracut, Germany). Because the balsa wood is very soft especially after treatment with fungus, it is very challenging to cut smooth cross sections. We immersed the samples into water first and then put into the fridge to freeze them to provide sufficient mechanical support of the wood during the cutting, which only served for taking SEM images.

Scanning electron microscopy

Wood samples were cut into smaller size of 5 mm by 5 mm by 5 mm. Then, they were put into the vacuum oven under 103°C for 12 hours for drying. Afterward, the wood samples were coated with Pt-Pd (80/20) by using a sputter coater (CCU-010, Safematic, Switzerland) to produce a coating of about 10 nm to make the surface conductive. The structure of the samples was characterized by field-emission SEM (FEI Quanta 200F).

Fourier transform infrared spectroscopy

Thin slices of wood samples were analyzed with an FTIR spectrometer (Bruker Tensor 27) over the scan range of 400 to 4000 cm^{-1} to see the changes in chemical composition of the cell walls upon fungal treatment. The spectra were normalized (min/max) and baseline-corrected in the OPUS software and plotted in OriginPro 8.6.

Measurement of electrical output

First, two pieces of copper foil with a size of 15 mm by 15 mm were attached onto the radial sections of the wood block [15 mm (L) by 15 mm (R) by 15 or 13.2 mm (T)], which were then covered with two pieces of insulating substrate (e.g., wood veneer, 500-μm thick). Conductive wires were led out between the copper foil and wood veneer. Then, the sample was attached on a plate equipped with a loading cell (Model 31E mid.; maximum load, 50 N), mounted on the rigid frame of the motor to monitor the pressure applied on the samples. A linear motor (PL01-28x500/420) was used to apply a fixed pressure on the samples at constant frequency. The conductive wires were connected to a programmable electrometer (Keithley 6514), and the electrical output of native wood and decayed wood was measured by Keithley 6514 equipped with MATLAB software (fig. S5 illustrates the related assessment setup).

Further characterization techniques

The nanostructure of cellulose was studied by XRD (Panalytical X'Pert PRO MPD) using Cu Kα radiation (λ = 1.5406 Å). Mechanical properties of the samples were evaluated by using a universal mechanical testing machine (Shimadzu AGS-X, Japan), equipped with a 100-N load cell.

SUPPLEMENTARY MATERIALS

Supplementary material for this article is available at http://advances.sciencemag.org/cgi/content/full/7/11/eabd9138/DC1

REFERENCES AND NOTES

1. C. Ballif, L. E. Perret-Aebi, S. Lufkin, E. Rey, Integrated thinking for photovoltaics in buildings. *Nat. Energy* **3**, 438–442 (2018).
2. B. Svetozarevic, M. Begle, P. Jayathissa, S. Caranovic, R. F. Shepherd, Z. Nagy, I. Hischier, J. Hofer, A. Schlueter, Publisher Correction: Dynamic photovoltaic building envelopes for adaptive energy and comfort management. *Nat. Energy* **4**, 719–719 (2019).
3. P. Farese, How to build a low-energy future. *Nature* **488**, 275–277 (2012).
4. D. M. Kammen, D. A. Sunter, City-integrated renewable energy for urban sustainability. *Science* **352**, 922–928 (2016).
5. J. Rogelj, G. Luderer, R. C. Pietzcker, E. Kriegler, M. Schaeffer, V. Krey, K. Riahi, Correction: Energy system transformations for limiting end-of-century warming to below 1.5°C. *Nat. Clim. Change* **6**, 538 (2016).

6. S. B. Sadineni, S. Madala, R. F. Boehm, Passive building energy savings: A review of building envelope components. *Renew. Sustain. Energy Rev.* **15**, 3617–3631 (2011).
7. L. Gustavsson, A. Joelsson, Life cycle primary energy analysis of residential buildings. *Energ. Buildings* **42**, 210–220 (2010).
8. T. Li, Y. Zhai, S. M. He, W. T. Gan, Z. Y. Wei, M. Heidarinejad, D. Dalgo, R. Y. Mi, X. P. Zhao, J. W. Song, J. Q. Dai, C. J. Chen, A. Aili, A. Vellore, A. Martini, R. G. Yang, J. Srebric, X. B. Yin, L. B. Hu, A radiative cooling structural material. *Science* **364**, 760–763 (2019).
9. G. A. Barron-Gafford, M. A. Pavao-Zuckerman, R. L. Minor, L. F. Sutter, I. Barnett-Moreno, D. T. Blackett, M. Thompson, K. Dimond, A. K. Gerlak, G. P. Nabhan, J. E. Macknick, Agrivoltaics provide mutual benefits across the food-energy-water nexus in drylands. *Nat. Sustain.* **2**, 848–855 (2019).
10. M. H. Rafiei, H. Adeli, Sustainability in highrise building design and construction. *Struct. Des. Tall Spec.* **25**, 643–658 (2016).
11. J. Yan, Y. Yang, P. Campana, J. He, City-level analysis of subsidy-free solar photovoltaic electricity price, profits and grid parity in China. *Nat. Energy* **4**, 709–717 (2019).
12. B. P. Jelle, C. Breivik, H. D. Røkenes, Building integrated photovoltaic products: A state-of-the-art review and future research opportunities. *Solar Energ. Mater. Solar C.* **100**, 69–96 (2012).
13. T. N. Anderson, M. Duke, G. L. Morrison, J. K. Carson, Performance of a building integrated photovoltaic/thermal (BIPVT) solar collector. *Solar Energ.* **83**, 445–455 (2009).
14. G. Wimmers, Wood: A construction material for tall buildings. *Nat. Rev. Mater.* **2**, 17051 (2017).
15. E. Fukada, Piezoelectricity of wood. *J. Physical Soc. Japan* **10**, 149–154 (1955).
16. E. Fukada, Piezoelectricity as a fundamental property of wood. *Wood Sci. Technol.* **2**, 299–307 (1968).
17. M. H. Shamos, L. S. Lavine, Piezoelectricity as a fundamental property of biological tissues. *Nature* **213**, 267–269 (1967).
18. R. Mäkipää, T. Rajala, D. Schigel, K. T. Rinne, T. Pennanen, N. Abrego, O. Ovaskainen, Interactions between soil- and dead wood-inhabiting fungal communities during the decay of Norway spruce logs. *ISME J.* **11**, 1964–1974 (2017).
19. D. Floudas, M. Binder, R. Riley, K. Barry, R. A. Blanchette, B. Henrissat, A. T. Martinez, R. Otillar, J. W. Spatafora, J. S. Yadav, A. Aerts, I. Benoit, A. Boyd, A. Carlson, A. Copeland, P. M. Coutinho, R. P. de Vries, P. Ferreira, K. Findley, B. Foster, J. Gaskell, D. Glotzer, P. Gorecki, J. Heitman, C. Hesse, C. Hori, K. Igarashi, J. A. Jurgens, N. Kallen, P. Kersten, A. Kohler, U. Kues, T. K. A. Kumar, A. Kuo, K. LaButti, L. F. Larrondo, E. Lindquist, A. Ling, V. Lombard, S. Lucas, T. Lundell, R. Martin, D. J. McLaughlin, I. Morgenstern, E. Morin, C. Murat, L. G. Nagy, M. Nolan, R. A. Ohm, A. Patyshakuliyeva, A. Rokas, F. J. Ruiz-Duenas, G. Sabat, A. Salamov, M. Samejima, J. Schmutz, J. C. Slot, F. S. John, J. Stenlid, H. Sun, S. Sun, K. Syed, A. Tsang, A. Wiebenga, D. Young, A. Pisabarro, D. C. Eastwood, F. Martin, D. Cullen, I. V. Grigoriev, D. S. Hibbett, The paleozoic origin of enzymatic lignin decomposition reconstructed from 31 fungal genomes. *Science* **336**, 1715–1719 (2012).
20. M. Nofal, K. Kumaran, Biological damage function models for durability assessments of wood and wood-based products in building envelopes. *Eur. J. Wood Wood Prod.* **69**, 619–631 (2011).
21. M. A. Hulme, J. K. Shields, Biological control of decay fungi in wood by competition for non-structural carbohydrates. *Nature* **227**, 300–301 (1970).
22. T. P. Schultz, D. D. Nicholas, A. F. Preston, A brief review of the past, present and future of wood preservation. *Pest Manag. Sci.* **63**, 784–788 (2007).
23. The testing of wood preservatives. *Nature* **126**, 921–922 (1930).
24. R. A. Blanchette, L. Otjen, M. J. Effland, W. E. Eslyn, Changes in structural and chemical-components of wood delignified by fungi. *Wood Sci. Technol.* **19**, 35–46 (1985).
25. D. Martinez, L. F. Larrondo, N. Putnam, M. D. S. Gelpke, K. Huang, J. Chapman, K. G. Helfenbein, P. Ramaiya, J. C. Detter, F. Larimer, P. M. Coutinho, B. Henrissat, R. Berka, D. Cullen, D. Rokhsar, Genome sequence of the lignocellulose degrading fungus *Phanerochaete chrysosporium strain RP78*. *Nat. Biotechnol.* **22**, 695–700 (2004).
26. K. K. Pandey, A. J. Pitman, FTIR studies of the changes in wood chemistry following decay by brown-rot and white-rot fungi. *Int. Biodeter. Biodegr.* **52**, 151–160 (2003).
27. T. Nakai, N. Igushi, K. Ando, Piezoelectric behavior of wood under combined compression and vibration stresses I: Relation between piezoelectric voltage and microscopic deformation of a Sitka spruce (*Picea sitchensis* Carr.). *J. Wood Sci.* **44**, 28–34 (1998).
28. T. Nakai, K. Ando, Piezoelectric behavior of wood under combined compression and vibration stresses—II: Effect of the deformation of cross-sectional wall of tracheids on changes in piezoelectric voltage in linear-elastic region. *J. Wood Sci.* **44**, 255–259 (1998).
29. J. G. Sun, H. Y. Guo, J. Ribera, C. S. Wu, K. K. Tu, M. Binelli, G. Panzarasa, F. Schwarze, Z. L. Wang, I. Burgert, Sustainable and biodegradable wood sponge piezoelectric nanogenerator for sensing and energy harvesting applications. *ACS Nano* **14**, 14665–16474 (2020).
30. P. MacNaughton, X. Cao, J. Buonocore, J. Cedeno-Laurent, J. Spengler, A. Bernstein, J. Allen, Energy savings, emission reductions, and health co-benefits of the green building movement. *J. Expo. Sci. Environ. Epidemiol.* **28**, 307–318 (2018).
31. R. L. Fares, M. E. Webber, The impacts of storing solar energy in the home to reduce reliance on the utility. *Nat. Energy* **2**, 17001 (2017).
32. S. Chu, A. Majumdar, Opportunities and challenges for a sustainable energy future. *Nature* **488**, 294–303 (2012).
33. J. Kan, R. J. Ross, X. W. Wang, W. B. Li, Energy harvesting from wood floor vibration using a piezoelectric generator, in *Research Note FPL–RN–0347* (U.S. Department of Agricuture, Forest Service, Forest Products Laboratory, 2017).
34. C. H. Yao, A. Hernandez, Y. H. Yu, Z. Y. Cai, X. D. Wang, Triboelectric nanogenerators and power-boards from cellulose nanofibrils and recycled materials. *Nano Energy* **30**, 103–108 (2016).
35. M. Borrega, P. Ahvenainen, R. Serimaa, L. Gibson, Composition and structure of balsa (*Ochroma pyramidale*) wood. *Wood Sci. Technol.* **49**, 403–420 (2015).
36. F. Schwarze, Wood decay under the microscope. *Fungal Biol. Rev.* **21**, 133–170 (2007).
37. M. Frey, D. Widner, J. S. Segmehl, K. Casdorff, T. Keplinger, I. Burgert, Delignified and densified cellulose bulk materials with excellent tensile properties for sustainable engineering. *ACS. Appl. Mater. Inter.* **10**, 5030–5037 (2018).
38. H. Guan, Z. Y. Cheng, X. Q. Wang, Highly compressible wood sponges with a spring-like lamellar structure as effective and reusable oil absorbents. *ACS Nano* **12**, 10365–10373 (2018).
39. L. Qiu, J. Z. Liu, S. L. Y. Chang, Y. Z. Wu, D. Li, Biomimetic superelastic graphene-based cellular monoliths. *Nat. Commun.* **3**, 1241 (2012).
40. H. Hu, Z. Zhao, W. Wan, Y. Gogotsi, J. Qiu, Ultralight and highly compressible graphene aerogels. *Adv. Mater.* **25**, 2219–2223 (2013).
41. M. Vural, G. Ravichandran, Microstructural aspects and modeling of failure in naturally occurring porous composites. *Mech. Mater.* **35**, 523–536 (2003).
42. A. Da Silva, S. Kyriakides, Compressive response and failure of balsa wood. *Int. J. Solids Struct.* **44**, 8685–8717 (2007).
43. N. Hirai, N. Sobue, M. Date, New piezoelectric moduli of wood: d 31 and d 32. *J. Wood Sci.* **57**, 1–6 (2011).
44. S. A. Han, T.-H. Kim, S. K. Kim, K. H. Lee, H.-J. Park, J.-H. Lee, S.-W. Kim, Point-defect-passivated MoS_2 nanosheet-based high performance piezoelectric nanogenerator. *Adv. Mater.* **30**, e1800342 (2018).
45. K. Y. Lee, J. Bae, S. Kim, J. H. Lee, G. C. Yoon, M. K. Gupta, S. Kim, H. Kim, J. Park, S. W. Kim, Depletion width engineering via surface modification for high performance semiconducting piezoelectric nanogenerators. *Nano Energy* **8**, 165–173 (2014).
46. S. S. Kwak, S. M. Kim, H. Ryu, J. Kim, U. Khan, H. J. Yoon, Y. H. Jeong, S. W. Kim, Butylated melamine formaldehyde as a durable and highly positive friction layer for stable, high output triboelectric nanogenerators. *Energ. Environ. Sci.* **12**, 3156–3163 (2019).
47. R. Hinchet, U. Khan, C. Falconi, S.-W. Kim, Piezoelectric properties in two-dimensional materials: Simulations and experiments. *Mater. Today* **21**, 611–630 (2018).

Acknowledgments: We thank Z. Lin Wang and C. Wu for providing useful suggestions for establishing the electrical output measuring system. We thank T. Schnider for the wood sample preparation. **Funding:** There is no funding to declare. **Author contributions:** J.S., H.G., I.B., and J.R. conceived the study. J.S., J.R., G.N.S., K.T., and S.S. performed experiments and analyzed data. J.S., G.P., I.B., and J.R. cowrote the manuscript. All authors discussed the results and commented on the manuscript. **Competing interests:** The authors declare that they have no competing interests. **Data and materials availability:** All data needed to evaluate the conclusions in the paper are present in the paper and/or the Supplementary Materials. Additional data related to this paper may be requested from the authors.

Submitted 20 July 2020
Accepted 20 November 2020
Published 10 March 2021
10.1126/sciadv.abd9138

Citation: J. Sun, H. Guo, G. N. Schädli, K. Tu, S. Schär, F. W. Schwarze, G. Panzarasa, J. Ribera, I. Burgert, Enhanced mechanical energy conversion with selectively decayed wood. *Sci. Adv.* **7**, eabd9138 (2021).

Science Advances

Enhanced mechanical energy conversion with selectively decayed wood

Jianguo Sun, Huizhang Guo, Gian Nutal Schädli, Kunkun Tu, Styfen Schär, Francis W.M.R. Schwarze, Guido Panzarasa, Javier Ribera and Ingo Burgert

Sci Adv **7** (11), eabd9138.
DOI: 10.1126/sciadv.abd9138